

Cosmic Muons Scattering in MicroBooNE
MPhys Project Report

Kang Yang
18th December 2018

Supervisor: Dr.Justin Evans, Dr.Andrew Furmanski

Abstract

A Corsika Monte Carlo simulation sample of 63456 cosmic events is used for the search of the cosmic muons scatter off argon nuclei. 434 interesting events are obtained by applying the pre-selection cut and the proton momentum threshold cut further reduces the sample size to 261. The performance of the PandoraCosmic package is tested on different reconstruction stages. In conclusion, PandoraCosmic is able to identify cosmic muon scattering events, but cannot provide the complete event reconstruction.

Acknowledgements

First and foremost, I would like to thank my supervisors Dr.Justin Evans and Dr.Andrew Furmanski. Thanks for your support and guidance throughout this project. Thank you to my partner Mathew Birch.

Contents

Abstract	i
Acknowledgements	i
List of Figures	iii
List of Tables	iii
1 Introduction	1
1.1 Neutrinos in Standard Model	1
1.2 Neutrinos Oscillation	1
1.3 Evidence for Sterile Neutrinos	2
1.3.1 LSND experiment	2
1.3.2 MiniBooNE experiment	2
1.4 Outline of this report	3
2 MicroBooNE Experiment	3
2.1 Experiment Overview	3
2.2 Liquid Argon Time Projection Chamber	4
2.3 Pandora Multi-algorithm Pattern Recognition	6
2.4 Motivation of This Project	7
3 Analysis of Monte Carlo Simulation	7
3.1 Cosmic Muon Scattering Event Selection	7
3.2 Investigation of Reconstructed Hits	9
3.2.1 Momentum Threshold Determination	9
3.2.2 Proton Energy Loss	10
4 Event Display in MicroBooNE	11
4.1 Event Display Overview	11
4.2 Event Display Examples	11
5 Conclusion	13
6 Further Work	14
References	14

List of Figures

1	The arrangement of the MicroBooNE experiment	4
2	Coordinate system used in the MicroBooNE experiment	4
3	The arrangement of the MicroBooNE LArTPC	5
4	2D Cluster Producing Algorithm	6
5	Theta Angle Distribution of Muons and Leading Protons	8
6	Phi Angle Distribution of Muons and Leading Protons	8
7	Purity Against Momentum	9
8	Average Hits Purity Before and After the Momentum Threshold Cut	10
9	Quality of Hits Before and After the Momentum Threshold Cut	10
10	The Geometric Demonstration of How to Calculate the Energy Loss	11
11	Example of the Bragg Peak of the Proton	11
12	Event Display Example 1	12
13	Event Display Example 2	13

List of Tables

1	The Pre-selection Cuts	8
---	----------------------------------	---

1 Introduction

1.1 Neutrinos in Standard Model

The neutrino was first postulated by Wolfgang Pauli in 1930 to explain how the beta decay can conserve the energy and momentum. The Beta decay is a process that a neutron decays into a proton and an electron (plus an antineutrino),

$$n \rightarrow p + e^- + \bar{\nu}_e \quad (1.1)$$

Being only weakly interacting, nearly massless and electrical neutral, neutrino was extremely difficult to detect at that time and many physicists believed this particle can never be detected. However, that changed when $\bar{\nu}_e$ was first observed by Reines and Cowan in 1956 [1]. They observed $\bar{\nu}_e$ via the inverse beta decay as,

$$\bar{\nu}_e + p \rightarrow n + e^+ \quad (1.2)$$

There are three flavours of neutrinos, ν_e , ν_μ , and ν_τ in the Standard Model and they are originally assumed to be massless in order to provide a convenient explanation for the parity violation in the weak interaction. In the famous Wu's experiment, she demonstrated that the parity conservation is maximally violated in the weak interaction. This result implied that the W boson only coupled to the left-handed (chirality) fermion and right-handed (chirality) anti-fermion. The chirality is a property of the particle and it cannot be measured directly in the experiment. Instead, a quantity called helicity which is related to chirality is measured. The helicity is defined as the projection of particle's spin vector to its momentum vector. However, the helicity of a massive particle is not uniquely defined since one can always find a reference frame to reverse the momentum vector of the particle, therefore change its helicity. Subsequent experiments showed that all neutrinos have their projected spin vector anti-aligned with momentum vector and the opposite for all anti-neutrinos. This implied that neutrinos must be massless, since in this limit, the helicity is equivalent to chirality.

This simple picture of neutrinos did not last long, as it cannot explain the “solar neutrino problem”. If the solar model was believed to be correct, then one will see more neutrinos coming from the sun, but actually only one third of the expected number of neutrinos were observed [2]. Therefore, one of the models must be wrong. It turns out that neutrinos are more complicated than other elementary particles.

1.2 Neutrinos Oscillation

The “solar neutrino problem” can be solved if one accept that neutrinos have mass and their flavour will oscillate as they travel through space and matter. In the current neutrino oscillation model, the neutrino flavour eigenstates are a rotation of three definite mass states described by the Pontecorvo–Maki–Nakagawa–Sakata matrix [3]. However, in most cases, only two neutrinos are involved in the oscillation, therefore in the two-neutrino oscillation approximation, the probability for one neutrino to change its flavour is

$$P_{\alpha \rightarrow \beta, \alpha \neq \beta} = \sin^2(2\theta) \sin^2(1.27 \Delta m^2 L_\nu / E_\nu), \quad (1.3)$$

where α, β are the neutrino flavour eigenstates, θ is the mixing angle between the mass eigenstates, $\Delta m^2(\text{eV}^2/\text{c}^4)$ is the difference in neutrino mass eigenstates squared, $L_\nu(\text{m})$ is the distance travelled by the neutrino, and $E_\nu(\text{MeV})$ is the neutrino energy. In this representation, the $\sin^2(2\theta)$ and the $\sin^2(1.27\Delta m^2 L_\nu / E_\nu)$ expressed the amplitude and the period of the oscillation respectively. Therefore, the mixing angle θ and the module of the mass difference squared between the definite mass eigenstates Δm^2 can be deduced by measuring the L_ν/E_ν . The observed oscillation parameters are:

$$\begin{aligned}\Delta m_{21}^2 &= \Delta m_{sol}^2 = (7.53 \pm 0.18) \times 10^{-5} \text{ eV}^2, \\ \Delta m_{32}^2 &= \Delta m_{atm}^2 = (2.44 \pm 0.06) \times 10^{-3} \text{ eV}^2 \\ \sin^2 2\theta_{12} &= \sin^2 2\theta_{sol} = 0.846 \pm 0.021 \\ \sin^2 2\theta_{23} &= \sin^2 2\theta_{atm} > 0.92, \text{ at } 90\% \text{ confidence level} \\ \sin^2 2\theta_{13} &= 0.0932 \pm 0.008\end{aligned}\tag{1.4}$$

where Δm_{21}^2 and $\sin^2 2\theta_{12}$ are measured by solar neutrino experiments, Δm_{32}^2 and $\sin^2 2\theta_{23}$ are measured by atmospheric neutrino experiments [4] and the last mixing angle is measured by experiments Daya Bay, Double Chooz and RENO [5].

1.3 Evidence for Sterile Neutrinos

1.3.1 LSND experiment

In the 1990s, the Liquid Scintillator Neutrino Detector (LSND) experiment was carried out at the Los Alamos National Laboratory. The primary aim of the LSND experiment was to search for $\bar{\nu}_\mu \rightarrow \bar{\nu}_e$ oscillations. A 798 MeV proton beam was used to initial a hadronic cascade on targets. The neutrino fluxes with energies between 20 and 52 MeV were dominantly produced by the π^+ and μ^+ decay at rest [6]. The detector was placed 30 meters away from the targets with a value of $L_\nu/E_\nu \sim 1\text{m}/\text{MeV}$ that is sensitive to $\Delta m^2 \sim 1\text{eV}^2$. The $\bar{\nu}_e$ was detected via a quasi-elastic Charge Current event as shown in Eq.1.2, this process provided a two-fold signature in the detector, a burst Cherenkov light from the outgoing electron and a delayed 2.2 MeV γ from a neutron capture process $n + p \rightarrow d + \gamma$.

The LSND collaboration claimed an excess of the $\bar{\nu}_e$ appearance events with the significance of 3.8σ . The unexpected excess of $\bar{\nu}_e$ events over the background cannot be explained by the three-neutrino oscillation model, as one has measured that $\Delta m_{21}^2 \sim 10^{-5}\text{eV}^2$ and $\Delta m_{32}^2 \sim 10^{-3}\text{eV}^2$. Therefore, some more exotic models need to be used. For example, there may exist some right-handed chirality sterile neutrinos that only interact with gravity. Also, it should be noted that there were many experiments showed null results in the range [7].

1.3.2 MiniBooNE experiment

The MiniBooNE (BooNE is an acronym for the Booster Neutrino Experiment) experiment was a Cherenkov detector, designed to confirm or refute the LSND anomaly. A 8 GeV proton beam was produced by the Booster Neutrino Beam (BNB) and interacted with a beryllium target in the magnetic horn. The neutrino and anti-neutrino mode can be switched on

and off by changing the magnetic field inside the target horn. The energies of ν_μ and $\bar{\nu}_\mu$ fluxes were peaked at approximately 600 MeV and 400 MeV respectively [8]. Furthermore, the MiniBooNE detector was placed 541m from the target horn which provided a similar $L_\nu/E_\nu \sim 1\text{m}/\text{MeV}$ as that in LSND. From 2002-2017, the MiniBooNE experiment had collected 11.27×10^{20} and 12.84×10^{20} protons on target in the anti-neutrino and neutrino mode respectively. The MiniBooNE collaboration reported an excess of ν_e events with a significance of 4.6σ in neutrino mode and the results from anti-neutrino mode was agreed with the LSND experiment. The significance of the combined LSND and MiniBooNE excesses was found to be 6.0σ [8].

However, one of the major drawbacks of the Cherenkov neutrino detector is the inability to distinguish electrons from photons, as they both produce the electromagnetic showers and are characterised as “fuzzy” rings in the detector. Even though a painstaking work have been done for discriminating the signal and the background, the results are still controversial in the community. Those difficulties can be resolved by the MicroBooNE experiment which is described in the following section.

1.4 Outline of this report

My MPhys project is focused on understanding inelastic muon scattering on argon producing protons in the final state using the cosmic muons events generated by Corsika Monte Carlo simulation. The outline of this report is as follow. I will describe the MicroBooNE experiment and its reconstruction packages in Section 2. Then, I will describe the outcomes by analysing the Monte Carlo simulation data in Section 3. Finally, I will discuss some examples of the event display in Section 4.

2 MicroBooNE Experiment

2.1 Experiment Overview

The MicroBooNE experiment employs a Liquid Argon Time Projection Chamber (LArTPC) as the detector because of its superior ability to separate the electron and photon events in a relatively low energy range. The primary aim of the MicroBooNE is to address the short baseline neutrino oscillation anomaly observed by both MiniBooNE and LSND experiments. The other physical goal of MicroBooNe is searching for the supernova and proton decay. The arrangement of the MicroBooNE experiment along the BNB beam line is shown in Fig.1. The MicroBooNE is located about 600m from the neutrino production target and the L_ν/E_ν value is the same as the MiniBooNE experiment. The LArTPC is exposed to a dense neutrino beam produced dominantly by the pion and muon decay chain initiated by the proton beam. The MicroBooNE began to collect data in late 2015 and aimed for a ~ 3 years run [9]. In 2018, the MicroBooNE will be employed as part of an expanded Short Baseline Neutrino program in Fermilab.

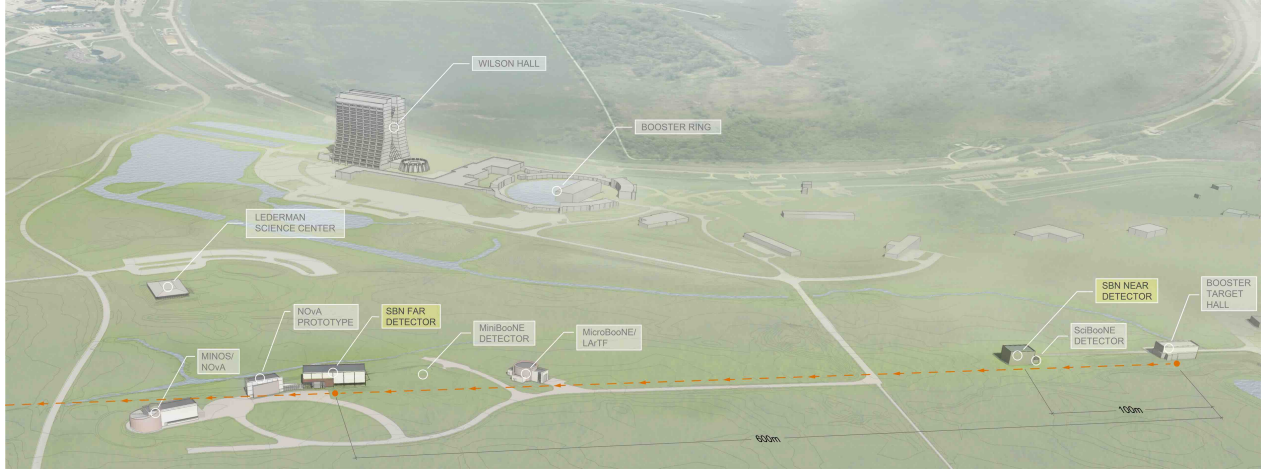


Figure 1: The arrangement of the MicroBooNE experiment along the BNB beam line (the orange dashed line) [9].

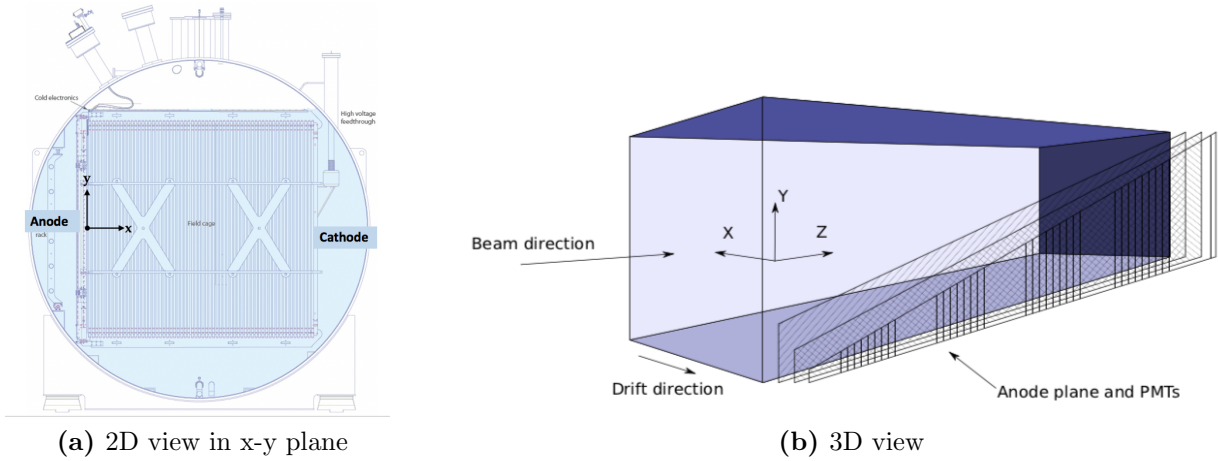


Figure 2: Coordinate system used in the MicroBooNE experiment [9][10].

2.2 Liquid Argon Time Projection Chamber

The Liquid Argon based technology was first developed in the ICARUS and ArgoNeuT experiments. The LArTPCs planned to play a important role in the next generation of the neutrino detectors. Besides the MicroBooNE, the Short Baseline Neutrino Detector (SBND) experiment and the Deep Underground Neutrino Experiment (DUNE) are being constructed now. The volume of the MicroBooNe LArTPC is $10\text{m} \times 2.2\text{m} \times 2.5\text{m}$ and contains 170 tons of liquid argon in total [9]. The MicroBooNE uses a right handed Cartesian coordinates as shown in Fig.2. The origin is located at the mid-point of the innermost anode plane (closest to the cathode). The positive z-axis is defined as the beam direction. The angle theta θ is defined as the angle from the beam-line in the y-z plane (i.e. $\theta = 0$ is along the beam line $\theta = \pi/2$ is perpendicular to the beam line) and and the angle phi ϕ is defined as the angle around the beam-line in the x-y plane (i.e. $0 < \phi < \pi$ is the upper volume and $0 < \phi < -\pi$ is the lower volume).

As charge particles transverse through the LArTPC, they ionise electrons along their trajectories and also produce the prompt vacuum ultraviolet (VUV) scintillation photons.

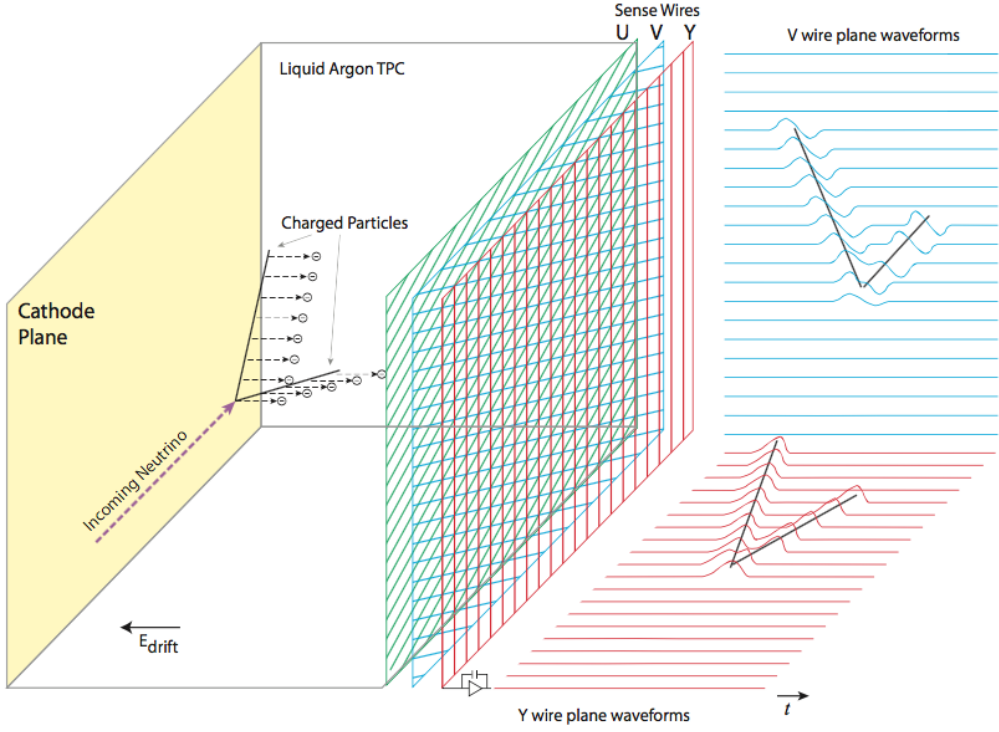


Figure 3: The arrangement of the MicroBooNE LArTPC and an example signal that is obtained on the anode plane [9].

These ionisation electrons are drifted by a constant electric field towards the anode. There are three wire planes on the anode for collecting these signals and the orientations are shown in Fig.3. The raw readout is the electric field measured by wires in each plane, as the ionisation electrons pass through the first two planes (labeled as U and V), they alter the measured electric field to produce a bipolar waveform (the signalling elements lie between some arbitrary positive and negative volts). Therefore, U and V planes are referred as induction planes and wires are orientated $\pm 60^\circ$ relative to the vertical. The electrons are finally collected by the Y plane to produce an unipolar waveform (the signalling elements lie between zero volts and some arbitrary positive volts). The Y plane is referred as the collection plane and wires are held in the vertical direction. Those waveforms are shown on the right-hand side of Fig.3. Whereas, the VUV photons are collected by 32 photomultiplier tubes (PMTs) located behind the three wire planes. The “fast” scintillation light provides a t_0 (event starting time) within a few nanoseconds and provides the trigger time of the event. Because both the event time and the electron drift time are on the order of microseconds, the t_0 also provides the information for the background rejection as there may be some external events overlapped within the beam window.

Since the MicroBooNE LArTPC is only 6m below the Earth’s surface, it is classified as a “surface detector” that exposed to cosmic rays. Due to the large readout window for collecting drifted electrons, there are approximately 15-24 cosmic muons transversing the LArTPC per each readout window [11]. Therefore, it is crucial to discriminate cosmic muon events from the beam neutrino induced events. The reconstruction of cosmic events is achieved by the PandoraCosmic package that will be discussed in Section 2.3.

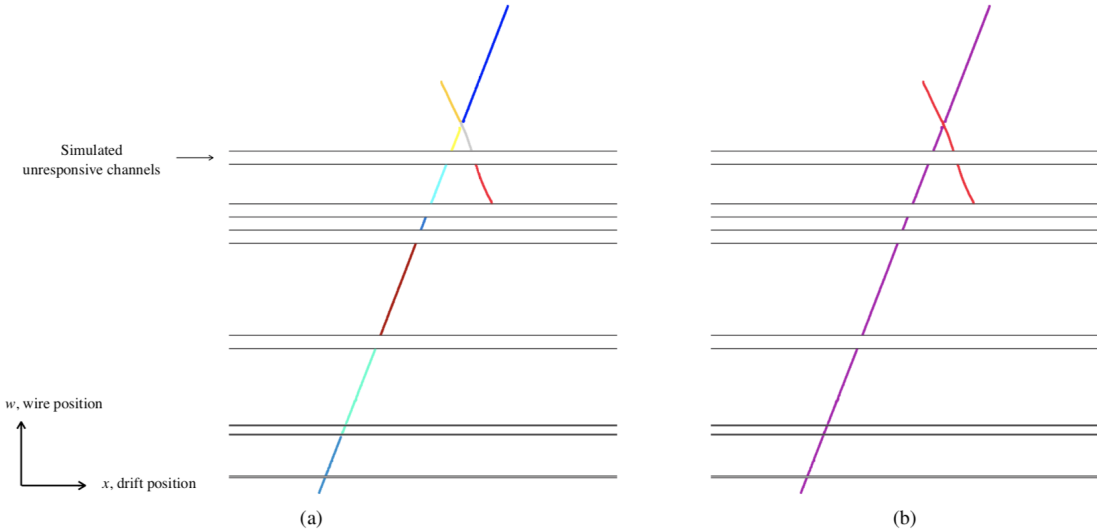


Figure 4: (a)Clusters produced by the ClusterCreation algorithm. (b) Completed clusters produced by the Cluster-merge algorithm [12].

2.3 Pandora Multi-algorithm Pattern Recognition

Pandora reconstruction packages are built within the LArSoft framework [12]. There are two existing Pandora reconstruction paths, PandoraCosmic (aimed to identify cosmic muons) and PandoraNu (optimised to identify neutrinos). Since typical energies of cosmic muons are quite high, they almost pass the entire TPC volume, therefore the PandoraCosmic is a strongly track-oriented package. On the other hand, neutrinos produce no tracks inside the TPC, all daughter particles of a neutrino come from a vertex. Hence, the PandoraNu is a vertex-oriented package and has capability to link daughter particles to the parent neutrino.

In the pre-reconstruction stage, all waveforms collected by three wire planes are fitted by a Gaussian distribution function to form a hit with a certain width. The overall reconstruction procedure in the MicroBooNe is that all hits are first passed to the PandoraCosmic, for those hits tagged as cosmic muon events will be removed, then a new set of cosmic-removed hits are created as the input for the PandoraNu reconstruction. Because this project is mainly focused on cosmic muon events, only the PandoraCosmic reconstruction package is discussed in this section.

The first stage in the reconstruction is to separate all input hits into three groups corresponds to three planes and this is achieved by the EventPreparation algorithm. For each wire plane, a line of continuous and unambiguous hits, referred as a 2D cluster, are produced by the ClusterCreation algorithm. If there is any bifurcation or ambiguity, then the current cluster stops and a new cluster is created to continue the clustering. This will provide several clusters with high purity, even though the completeness of clusters is low as shown in Fig.4(a). Then the Cluster-merge algorithm will improve the completeness by merging a pair of clusters that either close or point to each other as shown in Fig.4(b).

The second stage is to reconstruct 3D tracks using 2D clusters from three wire planes. Since the x-coordinate (drift time axis) of three planes are the same for an event, a sample region in x-coordinate can be defined in all three planes. Then by using the position of clusters from a pair of planes, the position of the cluster on the third plane can be predicted (i.e. $U, V \rightarrow Y; U, Y \rightarrow V; V, Y \rightarrow U$). If the prediction matches with the signal for all three configurations, then those three 2D clusters are collected together to produce a 3D track by the ClearTracks tool. However, if there are some ambiguities, for example in a given region of x, there is more than one cluster which means clusters are matched in multiple combinations, then the LongTracks tool is applied for the track reconstruction. Since there will be one of combinations that is better than others with larger x-overlap, this combination is used to create the 3D track of the particle by the LongTracks tool.

The third stage is the associated delta rays reconstruction. For those hits that are not participate in the previous stage but closed to the muon track, the DeltaRayMatching algorithm is used to merge the cluster from different views to form a delta ray and identify the appropriate parent muon.

2.4 Motivation of This Project

Since the LArTPC in the MicroBooNe is a surface detector, it exposed to abundant cosmic rays. Most cosmic muons transverse through the entire detector without any interactions and only produce some delta rays, the reconstruction of these kinds of events is well developed by the PandoraCosmic package. However, there are some events in which cosmic muons scatter off argon nuclei inelastically and produce several daughter particles. They are completely different event topology compared with neutrino induced scatters, but produce a rather similar final state (protons, neutrons and pions etc.). This project is mainly focused on scatter events that produce protons. These kinds of scatters should be classified as cosmic background by the algorithm. Therefore, the aim of this project is to test the feasibility of Pandora algorithm tools are available to reconstruct and remove Cosmic muon inelastic scattering events.

3 Analysis of Monte Carlo Simulation

3.1 Cosmic Muon Scattering Event Selection

A Corsika Monte Carlo simulation sample of 63456 events is generated for the search of a cosmic muon scatters off Argon nuclei. In order to select those events, protons need to come from the muon parent. Those events are labeled as “muonNuclear” in the MC simulation. The fiducial volume of the LArTPC in this experiment is defined as at least 10 cm from the edges in the x and z direction and 20 cm from the edges in the y direction. The proton tracks need to be inside the LArTPC to extract the full Bragg peak. Furthermore, the drifted time of ionised electrons need to be within the readout window for each measurable event. A summary of the above pre-selection is shown in Tab.1.

Table 1: Pre-Selection of cosmic muon scatter events

Requirement	
Event Process	“muonNuclear”
Fiducial Volume	$10 \text{ cm} < x < 250 \text{ cm}$ $-95 \text{ cm} < y < 95 \text{ cm}$ $10 \text{ cm} < z < 1030 \text{ cm}$
Proton tracks	inside the fiducial volume
Drift Time of Electrons	within the readout window

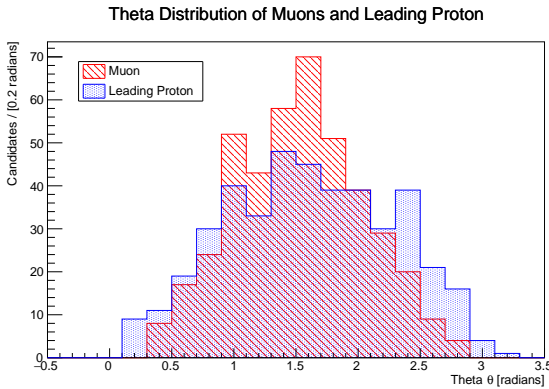


Figure 5: Theta angle distribution of muons and leading protons, the red histogram and the blue histogram represent muons and leading protons respectively.

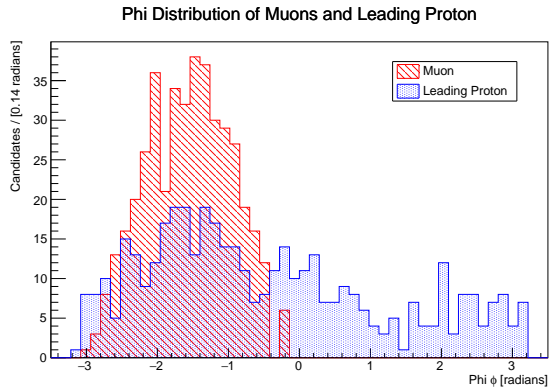


Figure 6: Phi angle distribution of muons and leading protons, the red histogram and the blue histogram represent muons and leading protons respectively.

There are 424 interesting events passed through the pre-selection cuts, and if more than one proton are produced after the scattering, only the leading proton is considered, defined as the proton with the highest momentum in the event. The theta angle of both muons and leading protons are shown in Fig.5. A peak around $\pi/2$ is found and indicated that muons and leading protons prefer to travel away from the beam-line (z-axis) rather than along it in either directions. The phi angle distribution is shown in Fig.6. For muons, the phi angle is confined in the range from 0 to $-\pi$ as they are coming from the atmosphere. For leading protons, the phi angle is more likely to be negative which suggests that they are more likely to travel downwards as expected.

Since the number of hits produced on the anode plane depend on the length of the track, and the greater momentum of the leading proton, the longer the track will be. Therefore, the momentum of proton need to be greater than a threshold value. Because the first few hits of the proton track are contributed not only by protons but also the muon and some secondary charged particles produced at the vertex. This momentum threshold is determined in Section 3.2.1 by investigating the hits purity.

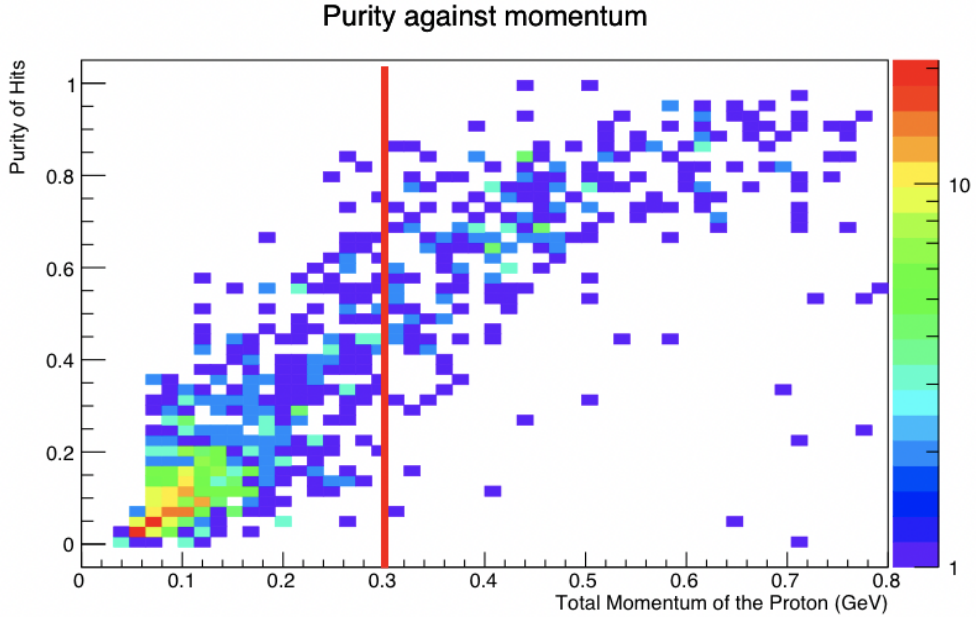


Figure 7: Average hits purity against the proton momentum, the red line represents the threshold cut on the momentum

3.2 Investigation of Reconstructed Hits

3.2.1 Momentum Threshold Determination

In order to obtain the momentum threshold, proton hits which produced in the pre-reconstruction stage are investigated. Since each hit is obtained by fitting a Gaussian distribution to the waveform collected on the wire plane, the variable defined as the fraction of the energy deposit by the particle that contribute to the waveform is called the hits purity. For each hit, the hits purity is a number between 0 and 1. If it is equal to 1, then it means that all the energy deposit in this hit is coming from one single particle. All 989 protons are examined in the 424 events sample and 47000 hits are obtained in all three wire planes. Each proton is comprised by a set of hits, the average hits purity is defined as the sum of the purity of each hit divided by the total number of hits in this set. The average hits purity against the proton momentum is shown in Fig.7. The x-axis shows momenta of protons in unit of GeV and the y-axis shows the average hits purity of protons. For the momentum below 0.3 GeV (indicated by the left-hand side of the red line on the graph), the average purity for most protons is below 0.4. Therefore, a 0.3 GeV threshold on the proton momentum is applied in order to make the reconstruction more accurate. The events sample is further reduced from 434 to 261.

For each set of hits, the number of hits that have purity above a certain value divided by the total number of hits reflects the quality of hits for this proton. Both the average hits purity and the hits quality are plotted in Fig.8 and Fig.9 respectively. The blue filled histogram and the red transparent histogram represent the data before and after applying the momentum threshold respectively. This threshold on proton momentum clearly increases the average purity and hits quality as the distribution is more concentrated on the range closed to one.

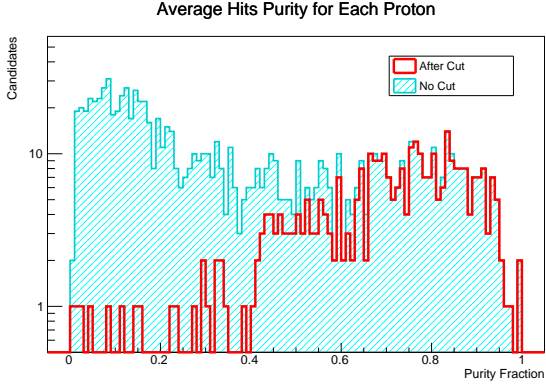


Figure 8: Average hits purity for protons before and after the momentum threshold cut

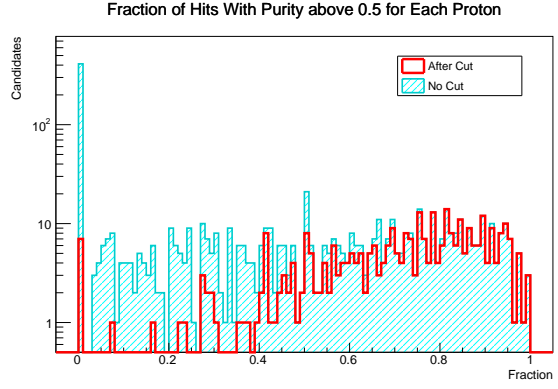


Figure 9: Quality of hits for each proton before and after the momentum threshold cut.

3.2.2 Proton Energy Loss

Since the proton has a larger mass compared with the electron, the ionisation energy loss is dominated as it travels in the detector. In particular, at the end of the track, the ionisation energy loss is maximal since dE/dx is inversely proportional to the velocity of the particle and this maximum is called the Bragg peak. Therefore, if proton hits are properly obtained in the pre-reconstruction stage, the Bragg peak should be seen if one plots the graph of the energy loss against the track length. The geometric demonstration of how to calculate the dE/dx is shown in Fig.10. This is an example of the Y plane view, vertical black lines are wires with a 3 mm pitch. Blue circles represent hits obtained on the wire and the orange line is the track of the particle. The normal unit vector is shown by a red dashed arrow which is along the positive z-axis direction. If the particle travels at an angle θ relative to the normal vector direction, then the dot product of the track vector and the normal vector can be computed and therefore the angle θ is obtained. Hence, the quantity $dx = 3\text{mm}/\cos\theta$ can be calculated. Since the track is not reconstructed yet in this stage, but the track information is needed in this calculation. Instead, the truth information of the track is used. Furthermore, the energy deposit (dE) of each hit is stored in the recob::hits reference class in unit of analogue to digital converter (ADC). The conversion of the energy from ADC unit to MeV unit can be found in [13].

Fig.11 shows an example of the Bragg peak of a single proton in one event. The y-axis is the dE/dx in the unit of ADC/cm and the x-axis is the residual range in unit of cm, defined as the distance relative to the end point of the track (i.e. $x = 0$ is the end point of the track). Fig.11 also reflects the fact that the energy deposit of the first few hits have poor quality as can be seen by the unexpected shape of the energy loss. Furthermore, a clear peak is found and dropped quickly at the end of the track. However, a much quicker drop is expected for the Bragg peak, this might due to the non-linearity relation between the energy in ADC unit and in MeV unit.

In conclusion, hits of the proton track that produced in the pre-reconstruction stage are reconstructed well by PandoraCosmic. The next step is to test the algorithm used in the 2D clusters stage and the 3D tracks stage of PandoraCosmic. This will be discussed in details in Section 4 through event display.

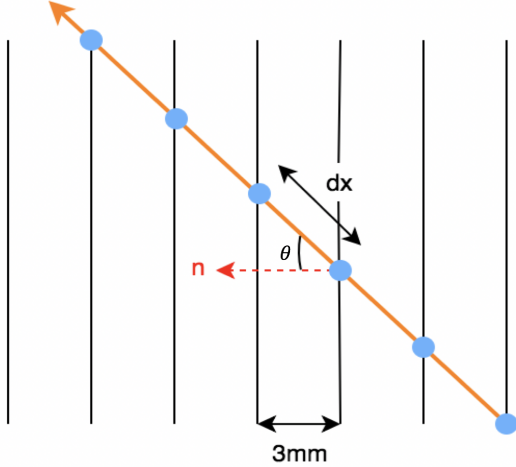


Figure 10: The geometric demonstration of how to calculate the energy loss.

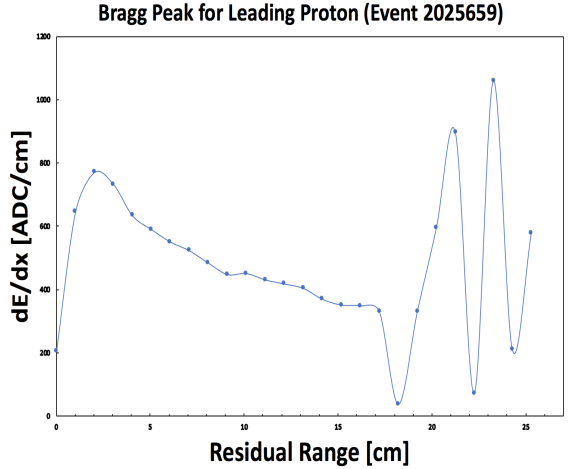


Figure 11: Example of the Bragg peak of the proton from muon scatter events.

4 Event Display in MicroBooNE

4.1 Event Display Overview

In this section, the outcomes of each stage produced by PandoraCosmic package is studied through the event display. The MC truth information is used to identify the particle in the raw wire data. For the views of each plane, the horizontal axis is the space coordinate and the vertical axis is the time coordinate. There are four types of data that can be displayed on each plane. The first is the raw wire data, the second is the reconstructed hits, the third is the reconstructed 2D clusters, the last one is the 2D projection of the reconstructed 3D tracks. The reconstruction algorithm is described in Section 2.3 and reconstructed hits are investigated in Section 3. This section is focused on the reconstruction of the 2D clusters stage and the 3D tracks stage of cosmic muon scatter events.

4.2 Event Display Examples

The same event that produced the proton Bragg peak is used for the event display. The V plane view is shown in the Fig.12. For the 2D clusters stage, different reconstructed clusters are shown in different colours. The algorithm incorrectly merged the proton cluster with the incoming muon cluster as shown in Fig.12 (c). The reason for this is because the outgoing proton is too close to the outgoing muon and aligned with the incoming muon. This kind of events are referred as “messy” events which are not suitable for the PandoraCosmic to correctly reconstruct the 2D cluster. For the 3D tracks stage, both the incoming muon and the outgoing proton tracks are disappeared as shown in Fig.12 (d).

In order to investigate the ability of PandoraCosmic to reconstruct proton 2D clusters, several “clean” events are studied, defined as events that only involve a muon scatters off argon nuclei and produces distinct protons in the final state. One example can be seen in Fig.13. In this event, the outgoing proton is well separated with the muon and the 2D cluster of proton is reconstructed correctly as shown in Fig.13 (c). However, there is still no

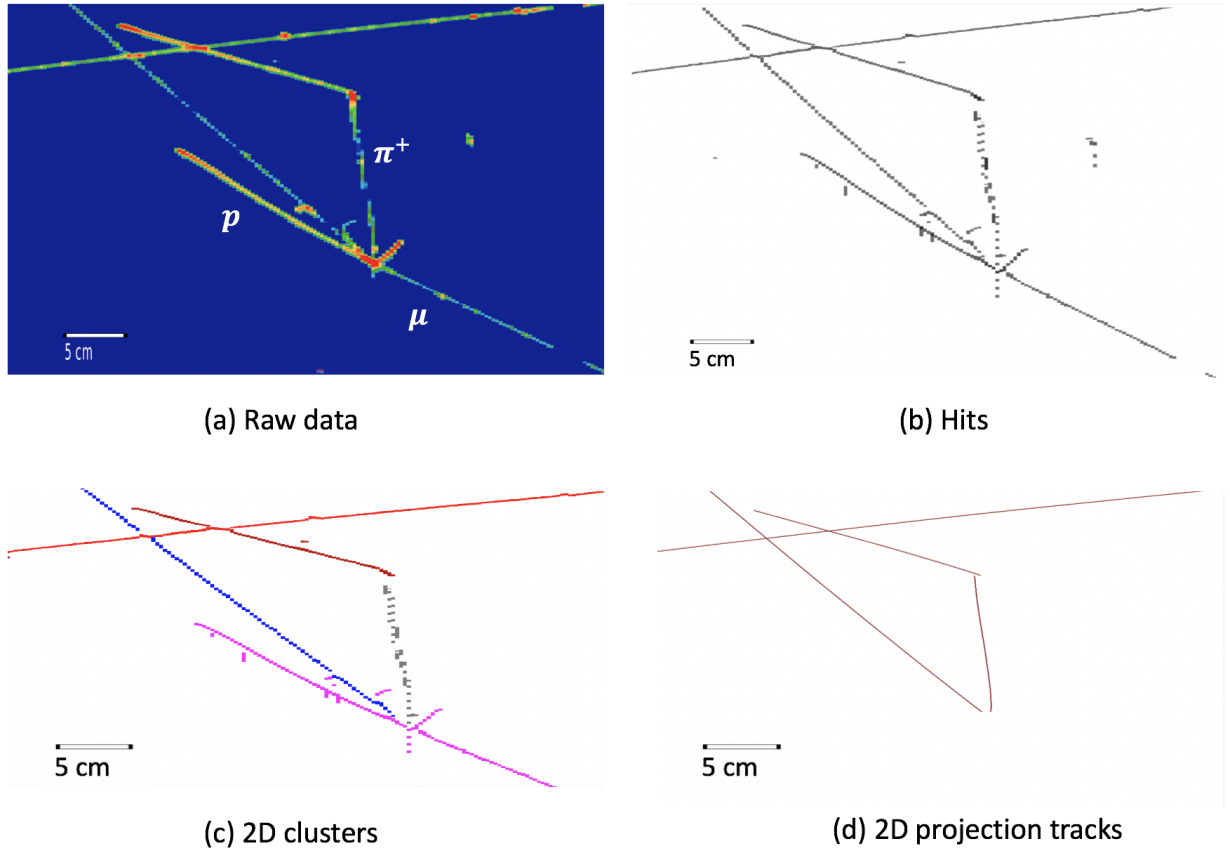


Figure 12: Event display of the event 2025659.

reconstructed track for the proton as shown in Fig.13 (d). The underlying reason for this can be ascribed to the 3D tracks reconstruction algorithm. The PandoraCosmic package is not design for the reconstruction of cosmic muon scattering events, but only for events that cosmic muons transverse the detector without any interactions. According to the LongTracks tool used in the 3D tracks reconstruction stage as described in Section 2.3, this tool will only use the better combination of clusters to reconstruct the particle track if there is more than one cluster in a given sample region in the x coordinate. Therefore, the longer track always wins since it has more x-overlap in a pair of planes. The remaining clusters that are not participate in the 3D tracks reconstruction go into the next delta ray reconstruction stage. The outcomes of this stage are not shown in the 3D tracks reconstruction and only labelled as daughter particles to the cosmic muon. That is the reason why the proton track disappears even though the 2D cluster is reconstructed correctly.

The set of hits that after the cosmic-tagged removal for several events have been checked, all the hits that come from the proton are removed along with muon hits. This is the expected result since cosmic muons and their daughter particles have to be removed to create a better environment for PandoraNu to reconstruct neutrino events. In conclusion, PandoraCosmic is able to remove all hits that come from cosmic muons and their daughter particles, but cannot provide the complete event reconstruction in muon scatter events.

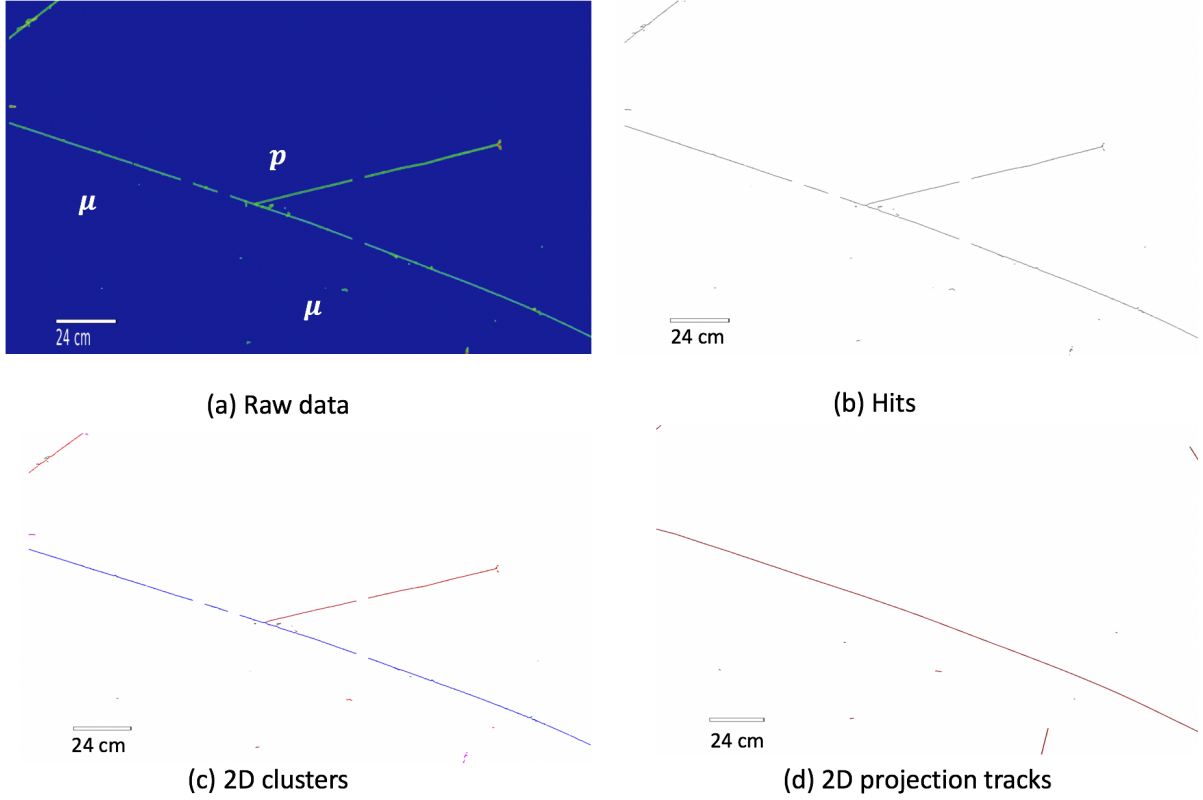


Figure 13: Event display of the event 2971309.

5 Conclusion

A Corsika Monte Carlo simulation sample of 63456 cosmic events is used for the search of cosmic muons scatter off argon nuclei. 434 interesting events are obtained by applying the pre-selection cut. Then the proton momentum threshold is determined by investigating the hits purity of each proton. This momentum threshold cut reduces the sample events to 261.

Furthermore, the performance of the next two stages, the 2D clusters and the 3D tracks, are checked through the event display. For those events which the outgoing proton is closed to the muon, reconstructed 2D clusters for protons are usually incorrect. For those events which the outgoing proton is well separated with the muon track, the distinct cluster can be reconstructed properly by PandoraCosmic. However, no proton tracks are reconstructed for both kinds of events. This is ascribed to the algorithm used in the 3D track reconstruction stage, since it is not designed for the muon scatter events. This does not affect the aim of the PandoraCosmic package, as it is able to remove almost all hits that come from muon daughter particles. Therefore, the set of remaining hits after the CosmicRemoval is almost zero for many sample events.

6 Further Work

Both cosmic muon transversing and muon scatter events inside the LArTPC can be identified and removed correctly by the PandoraCosmic package. However, PandoraCosmic cannot provide the complete event reconstruction for muon scatter events. If we want to get the whole event reconstruction including 3D tracks of all particles in the event, a different reconstruction package need to be used. The pmtrack package is one possible solution, but since the default input set of hits of pmtrack is the same as that in PandoraNu which is almost empty after the CosmicRemoval, the reconstruction ability cannot be tested. For the future work, we might change the default input and feed in original hits to pmtrack package to perform the reconstruction.

References

- [1] C. L. Cowan, F. Reines, F. B. Harrison, H. W. Kruse, and A. D. McGuire, “Detection of the free neutrino: a confirmation,” *Science*, vol. 124, no. 3212, pp. 103–104, 1956. [Online]. Available: <http://science.sciencemag.org/content/124/3212/103>
- [2] F. Kaether, W. Hampel, G. Heusser, J. Kiko, and T. Kirsten, “Reanalysis of the gallex solar neutrino flux and source experiments,” *Physics Letters B*, vol. 685, no. 1, pp. 47 – 54, 2010. [Online]. Available: <http://www.sciencedirect.com/science/article/pii/S0370269310000729>
- [3] Z. Maki, M. Nakagawa, and S. Sakata, “Remarks on the unified model of elementary particles,” *Progress of Theoretical Physics*, vol. 28, no. 5, pp. 870–880, 1962. [Online]. Available: <http://dx.doi.org/10.1143/PTP.28.870>
- [4] K. Olive and P. D. Group, “Review of particle physics,” *Chinese Physics C*, vol. 38, no. 9, p. 090001, 2014. [Online]. Available: <http://stacks.iop.org/1674-1137/38/i=9/a=090001>
- [5] K. Nakamura and P. D. Group, “Review of particle physics,” *Journal of Physics G: Nuclear and Particle Physics*, vol. 37, no. 7A, p. 075021, 2010. [Online]. Available: <http://stacks.iop.org/0954-3899/37/i=7A/a=075021>
- [6] A. Aguilar, L. B. Auerbach, R. L. Burman *et al.*, “Evidence for neutrino oscillations from the observation of $\bar{\nu}_e$ appearance in a $\bar{\nu}_\mu$ beam,” *Phys. Rev. D*, vol. 64, p. 112007, Nov 2001. [Online]. Available: <https://link.aps.org/doi/10.1103/PhysRevD.64.112007>
- [7] B. Armbruster, I. M. Blair, B. A. Bodmann *et al.*, “Upper limits for neutrino oscillations $\bar{\nu}_\mu \rightarrow \bar{\nu}_e$ from muon decay at rest,” *Phys. Rev. D*, vol. 65, p. 112001, Jun 2002. [Online]. Available: <https://link.aps.org/doi/10.1103/PhysRevD.65.112001>
- [8] A. A. Aguilar-Arevalo, B. C. Brown, L. Bugel *et al.*, “Significant excess of electronlike events in the miniboone short-baseline neutrino experiment,” *Phys. Rev. Lett.*, vol. 121, p. 221801, Nov 2018. [Online]. Available: <https://link.aps.org/doi/10.1103/PhysRevLett.121.221801>

- [9] R. Acciarri, C. Adams, R. An *et al.*, “Design and construction of the microboone detector,” *Journal of Instrumentation*, vol. 12, no. 02, p. P02017, 2017. [Online]. Available: <http://stacks.iop.org/1748-0221/12/i=02/a=P02017>
- [10] R. Acciarri, C. Adams *et al.*, “Measurement of cosmic-ray reconstruction efficiencies in the microboone larpc using a small external cosmic-ray counter,” *Journal of Instrumentation*, vol. 12, no. 12, p. P12030, 2017. [Online]. Available: <http://stacks.iop.org/1748-0221/12/i=12/a=P12030>
- [11] D. Kaleko, “Pmt triggering and readout for the microboone experiment,” *Journal of Instrumentation*, vol. 8, no. 09, p. C09009, 2013. [Online]. Available: <http://stacks.iop.org/1748-0221/8/i=09/a=C09009>
- [12] R. Acciarri, C. Adams, R. An *et al.*, “The pandora multi-algorithm approach to automated pattern recognition of cosmic-ray muon and neutrino events in the microboone detector,” *The European Physical Journal C*, vol. 78, no. 1, p. 82, Jan 2018. [Online]. Available: <https://doi.org/10.1140/epjc/s10052-017-5481-6>
- [13] R. Acciarri, C. Adams *et al.*, “Noise characterization and filtering in the microboone liquid argon tpc,” *Journal of Instrumentation*, vol. 12, no. 08, p. P08003, 2017. [Online]. Available: <http://stacks.iop.org/1748-0221/12/i=08/a=P08003>